Sensors & Actuators: B. Chemical 367 (2022) 132145

Contents lists available at ScienceDirect

Sensors and Actuators: B. Chemical

journal homepage: www.elsevier.com/locate/snb

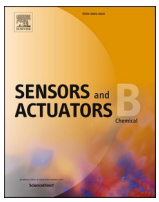

Functional fluorine-doped tin oxide coating for opto-electrochemical label-free biosensors

Dariusz Burnat [a], Petr Sezemsky [b], Katarzyna Lechowicz [a], Marcin Koba [a,c], Marta Janczuk-Richter [d], Monika Janik [a,e], Vitezslav Stranak [b], Joanna Niedziółka-Jönsson [d], Robert Bogdanowicz [e], Mateusz Śmietana [a,*]

[a] Warsaw University of Technology, Institute of Microelectronics and Optoelectronics, Koszykowa, 75, 00-662 Warszawa, Poland
[b] University of South Bohemia, Institute of Physics, Branisovska 1760, 370 05 Ceske Budejovice, Czech Republic
[c] National Institute of Telecommunications, Szachowa 1, 04-894 Warszawa, Poland
[d] Institute of Physical Chemistry, Polish Academy of Sciences, Kasprzaka 44/52, 01-224 Warszawa, Poland
[e] Gdansk University of Technology, Faculty of Electronics, Telecommunications and Informatics, Narutowicza 11/12, 80-233 Gdańsk, Poland

ARTICLE INFO

Keywords:
Fluorine-doped tin oxide (FTO)
Thin conductive oxides (TCO)
Optical fiber sensor
Lossy-mode resonance (LMR)
Electrochemistry
Label-free biosensing

ABSTRACT

Sensors operating in multiple domains, such as optical and electrochemical, offer properties making biosensing more effective than those working in a single domain. To combine such domains in one sensing device, materials offering a certain set of properties are required. Fluorine-doped tin oxide (FTO) thin film is discussed in this work as functional optically for guiding lossy modes and simultaneously electrochemically, i.e. as a conductive material for a working electrode. Performance of the FTO-based optical fiber lossy-mode resonance (LMR) sensor in both optical and electrochemical domains is analyzed. Additionally, to enhance applicability of the sensor, its probe-like reflection configuration has been developed. It is found that FTO may be considered as a promising alternative for other thin conductive oxides (TCO), such as indium tin oxide (ITO) that has been often applied up to date in various dual-domain sensing concepts. In the optical domain, the sensitivity of the FTO-LMR sensor to external refractive index (RI) has reached 450 nm/RIU in the RI range of 1.33–1.40 RIU. In the electrochemical domain, in turn, the response for FTO electrode in 1,1′-Ferrocenedimethanol solution has been reached with RedOx current low peak-to-peak separation. In contrast to the ITO-LMR sensors, the FTO-LMR counterparts exhibit a significant influence of applied potential on LMR wavelength shift in a wide potential range. It is shown using streptavidin as a target biomaterial that label-free biosensing applications of the FTO-LMR approach are possible. The dual-domain functionality allows for cross-verification between readouts received in both the domains, as well as enhancement of optical sensitivity when cross-domain interactions are applied.

1. Introduction

Ongoing COVID-19 pandemic revealed a demand for fast-responding, highly accurate, and reliable biosensing approaches. The sensors with such attributes can be obtained mainly using advanced, complex, and/or expensive technology [1,2] limiting their mass production and potential for wide application. When high accuracy and reliability are in particular expected, as an alternative to complex biosensing devices, those operating in multiple domains can be considered. Multi-domain sensors offer capability for application of different detection mechanisms using the same sensor at the same time. The approach allows for expansion of a measurement range [3], measurement of multiple parameters [4], or cross-verification of results obtained in the domains [5].

Biosensors may operate on basis of electrical, optical, chemical, mechanical, or thermal interactions [6]. In particular, sensors working in the optical domain make multiplexing possible and offer capacity for accurate, fast, and reliable analysis [6]. When label-free biosensing is considered, optical measurements focus on refractive index (RI) variation induced during specific binding of target molecules to receptor molecules at the sensor surface, i.e. formation of a thin film with the RI elevated versus the external medium [5–10]. Optical biosensors were recently applied in, e.g., cancer diagnosis [11], foodborne bacteria detection [12], or drug monitoring [13]. In turn, label-free biosensors

* Corresponding author.
E-mail address: M.Smietana@elka.pw.edu (M. Śmietana).

https://doi.org/10.1016/j.snb.2022.132145
Received 21 March 2022; Received in revised form 27 May 2022; Accepted 29 May 2022
Available online 1 June 2022

operating in the electrochemical (EC) domain rely on changes of electrical charge transfer at the sensor-electrolyte interface. When binding of receptor and target occurs, the charge transfer between the sensor's surface (electrode) and the electrolyte is disturbed. EC biosensors for DNA damage detection [14], breast cancer recognition [15], drug delivery systems [16] and other point of care testing [17] have already been reported. Merging EC and optical systems for label-free biosensing purposes is only possible for limited sensor material, i.e., materials showing electrical conductivity and optical transparency [18] or revealing additionally certain optical phenomena, such as surface plasmon resonance (SPR) [19]. In case of the SPR, binding between biological target and receptor occurs at the surface of typically gold electrode/sensor, therefore it modifies charge transfer, as well as changes RI there which disturbs surface plasmon propagation what can be monitored optically [20,21].

Previously reported dual-domain opto-EC sensors have employed different type of conductive waveguide structures, e.g., optical resonators etched in highly doped silicon layer (interferometer) [22], prism covered by metal film (SPR) [19] or planar optical waveguide covered by semiconducting film (evanescent field) [23]. Considering structures based on coated optical fiber, two optical phenomena were mainly studied, i.e., SPR, where gold film was employed [24–26], and less often lossy-mode resonance (LMR), where thin conductive oxide (TCO) such as indium tin oxide (ITO) film was used as a material supporting optical interactions [5,27]. Focusing on the latter, when ITO of a certain properties, i.e., high RI (around 2 in the spectral range of interrogation), nonzero extinction coefficient [28], and high enough thickness [29] is deposited on silica glass, the structure guides lossy modes in the visible (Vis) and infrared (IR) spectral range. The properties of the LMR depend on the RI of the external medium, as which can be considered biological layer bound to the film surface. ITO thin film, on top of high optical transparency, can be also conductive, EC-active, and can exhibit a wide EC potential window [27]. Except sensing applications, ITO is successfully used in displays and solar cells. However, ITO films show numerous limitations including brittleness, low stability at high temperature, and scarcity of indium resulting in high deposition costs [30,31]. Among the most significant limitations of ITO and silicon for their sensing applications are evolution of the film properties and their surfaces over time [32]. Thus, alternative materials capable of dual-domain (here optical and EC) sensing are sought for.

Fluorine-doped tin oxide (FTO) is an optically transparent material which has already been successfully applied as a working electrode in EC setups [33]. According to our best knowledge, in contrast to ITO, the material has been used in few optical sensing applications. So far FTO was reported for optical sensing as LMR-supporting material solely in [21], whereas TiO_2 [34], In_2O_3 [35], HfO_2, ZrO_2, Si_xN_y [36], various polymers [37], and ITO were the most often applied. The properties of FTO indicate that optically it can be considered as an alternative to the above-mentioned materials, and electrochemically as an alternative to ITO. FTO, similarly to ITO, is an optically transparent and high-RI material in the Vis and IR spectral range [38–40]. From the electrical point of view, FTO may offer low resistivity and fast electron transfer rates [41,42]. Moreover, FTO shows higher than ITO chemical, mechanical, and thermal stability, as well as it is less expensive in deposition [32,33,43,44]. These advantages over ITO indicate that FTO can be considered as a more promising material, especially for operating in chemically-aggressive solution or at elevated temperatures.

In this work, we optimize FTO properties for application of the material in double-domain, i.e. optical and EC sensing. Performance of the optimized material has been verified using a simple optical-fiber-based LMR device. Moreover, to increase the functional properties of the sensor and its applications in harsh environments, in contrast to standard transmissive sensor configuration, it was developed in a reflective scheme as an alternative. This probe-like approach allows for sensor miniaturization, i.e., the decrease of length of the sensor, and thus limitation of the volume of liquid required for analyses, as well as enhancement of the sensor functionality. Besides the introduction of additional technological steps, the sensor fabrication remains relatively simple, especially when compared to some other optical fiber sensors, such as gratings [45] or microcavities [46]. The FTO-based dual-domain sensing concept has been also verified for label-free sensing of streptavidin and in the future can be further extended to other biological or chemical targets.

2. Experimental details

2.1. Optical fiber processing

The sensors were prepared using polymer-clad silica multimode optical fiber (400/730 μm core/cladding) in two variants, i.e., transmissive and reflective. For transmissive samples we used 15-cm-long fibers, where the cladding was removed from their central section creating 2.5-cm-long part of the exposed core. Controlled chemical cladding removal was possible with dichloromethane. Reflective samples, in turn, had a 1.3 cm long exposed-core section and additionally an aluminum thin film deposited using DC magnetron sputtering on the cleaved end-faces on the exposed-core side. A 2-inch magnetron cathode with 99.999% purity Al target was used for deposition. The target was sputtered for 5 min with a power of 40 W and a pressure of 5 Pa controlled by Ar flow. The magnetron was supplied by ZZP4 – 05/P DC source provided by Institute for Sustainable Technologies, Poland.

2.2. Thin film deposition and characterization

The FTO deposition was performed by magnetron sputtering in the UHV chamber with base pressure in order of 10^{-5} Pa. A 3-inch FTO target was applied with a SnO_2:SnF_2 composition of 97:3 wt%. The sputtering cathode was driven by COMET Cito 1310 RF source (13.56 MHz, 150 W). During the deposition, the samples were rotated to ensure the maximum possible homogeneity of the coating around the exposed fiber core. To increase the temperature during the deposition an electrical heater was additionally installed in the chamber. The pressure of the Ar atmosphere in the chamber was set to 5 Pa to ensure sufficient heat transfer and enhanced homogeneity of the films due to increased diffusion of the sputtered species. Two alternative deposition configurations were tested, where the main difference between them was the distance between the sputtering source and fiber samples reaching 16 and 21 cm. Deposition configuration in the chamber has been described elsewhere [47].

To estimate RI of the films, i.e., its real (n) and imaginary part (k), as well as deposition rate, reference silicon wafers were prepared in separate processes, where deposition time was up to 100 min. The properties of the FTO films deposited on silicon wafers were identified using HORIBA Jobin Yvon UVISEL spectroscopic ellipsometer together with fitting to the New Amorphous and Drude thin film models. In addition, thickness of the thin film deposited directly on the optical fiber was estimated at cleaved FTO-coated optical fiber cross-section using Hitachi S-3400 scanning electron microscope (SEM).

2.3. Optical and EC measurements

The optical fiber samples were measured in the setup comprised of HL-2000 white light source and USB4000 spectrometer, both from Ocean Optics. The setup was kept simple, without any polarization managing devices although the spectral response of the LMR structure is polarization dependent and the magnitude and location of the minimum of the spectral response differ for each polarization. For the unpolarized light source and the multimode optical fiber the contributions of the polarizations superimpose [28] and the more pronounced resonance dip is observed and traced. Therefore, simple, robust, and experimentally proven concept was used. The optical spectra were recorded for samples surrounded by the air and water/glycerin solutions in different

proportions. The RI of the solutions (n_{ext}) was measured using Rudolph J57AB refractometer. All the obtained spectra were referred to the spectrum of an optical fiber prior to the film deposition (T-T_0). The RI sensitivity of FTO-coated sensor was defined as the LMR wavelength (λ_R) shift per RI unit (nm/RIU).

The EC activity of the FTO-LMR sensors was tested using a custom-made cell, where FTO played a role of a working electrode [27]. A copper tape was used to provide electrical contact to the sensitive region outside the cell. The remaining electrodes, i.e., counter and reference electrodes were platinum wire and Ag|AgCl|0.1 M NaCl, respectively. Cyclic voltammetry (CV) measurements were performed in 0.01 M phosphate-buffered saline (PBS, pH=7.0) and 1 mM 1,1′-Ferrocenedimethanol in 0.01 M PBS at different scan rates and potential ranges using PalmSens EmStat3+ potentiostat.

2.4. FTO surface functionalization and biosensing

To identify both EC and optical performance of the FTO-LMR approach for label-free biosensing applications, the surface of FTO has been modified towards the specific biding of an analyte. First, the FTO-LMR sensor was consecutively washed in isopropanol and water and dried in argon stream. Next, surface silanization with 3-aminopropyltriethoxysilane (APTES) was performed according to the procedure described in [48]. The reaction was carried out for 30 min and then the sample was left for 48 h under the argon atmosphere for curing of the silane layer. The deposited amine groups were activated by the glutaraldehyde (GLU) (Sigma-Aldrich) through immersion in 2.5% GLU solution in PBS for 30 min. Next, biotin (1 mg/mL dissolved in PBS) has been introduced as a recognition element. The sensor was immersed in the solution and left for 30 min at room temperature, then extensively washed with PBS. To prevent the non-specific interactions between FTO surface and target molecules, the sensor was immersed in a bovine serum albumin (BSA) solution (0.5 mg/mL in PBS) for 30 min and extensive washed with PBS. For the sensitivity analysis, the biotin-terminated sensor was incubated in elevating concentrations of streptavidin, i.e., 0.01, 0.1 and 1 mg/mL for 30 min in each the solution, and after each the concentration extensively washed with PBS. After each the incubation and washing, the sample have been analyzed in both PBS and 1 mM 1,1′-Ferrocenedimethanol in PBS using CV (4 cycles) at a scan rate of 20 mV/s in the potential ranging from − 0.2–1.0 V with simultaneous optical monitoring.

3. Results and discussion

3.1. Optical properties of the deposited FTO

Optical properties and thickness of the LMR-supporting thin film material are crucial for the performance of the sensors [37]. The dispersion curves of n and k for selected FTO films in the operational spectral range of the sensors are shown in Fig. 1. For all the cases at $\lambda <$ 400 nm the material shows high k, that corresponds to elevated absorption in the UV spectral range. Moreover, in this range also high changes of n are observed. Above that range, n and k change only slightly. In the IR range increase of k can be noticed and it corresponds to semi-metallic character of these films. Thus, it may be expected that the FTO thin films, similarly to some ITO films, can be used to obtain SPR in the IR. However, in the Vis range FTO is suitable for guiding lossy modes [28,49].

In general, it must be also noted that an increase of thickness of the FTO film leads to decrease in their n (Fig. 1(A)). In the case of In_2O_3 [50] and ITO [51] the trend is opposite, i.e., prolongation of deposition time results in increase of n. In turn, thermal post-processing may lead to decrease in n of In_2O_3 [52] and ITO [53]. For these materials decrease of n is correlated to lowering density of grains (crystals) in the film [51,52]. Deposition time and temperature of process can also change crystallinity and porosity of the material, therefore affect the n [54]. In this work, the deposition of FTO took place at elevated temperature, thus longer exposition of the sample could reduce n. Another possible reason of decreasing n is a stress in the film induced by the substrate [55]. Increasing deposition time and consequently the thickness of the film leads to intensification of the stress effect and reduction of n. A trend opposite to that of n is observed for k, i.e., for higher wavelengths k slightly increases (Fig. 1(B)). For other tin-oxide-based materials the deposition time or temperature, especially in the Vis range, rather did not show any clear impact on k [50–53,56,57].

From the LMR sensor performance point of view, drop of n of the film may be undesirable. Even though the LMR generation conditions are met, the RI sensitivity follows the n [37]. In turn, slight increase of k may promote deeper and well-pronounced LMR, but according to [29] the relation

$k < (\sqrt{2} - 1)n$ should be preserved. Thus, it must be taken into account that tuning of the deposition time has not only an effect on the film thickness, but also modifies optical properties of the FTO. On top of it, to effectively interrogate the sensor optically, the properties should be adjusted to meet requirements of the interrogation setup, such as its range and resolution.

The film thickness, next to its optical properties, is crucial for performance of the device. Estimated on the reference silicon wafers average deposition rate of FTO reached 1.8 nm/min. However, in the case of sputtering the rates on the flat silicon wafers and cylindrical optical fiber may differ as it was previously reported for ITO [27]. Hence, additional depositions on optical fiber were performed. The SEM images of the fibers cross-section were taken and shown in Fig. 2.

The SEM images reveals that the FTO deposition rate on the optical fiber are up to 5 times higher than for their counterpart deposited in the same conditions on the reference silicon wafers. This difference in

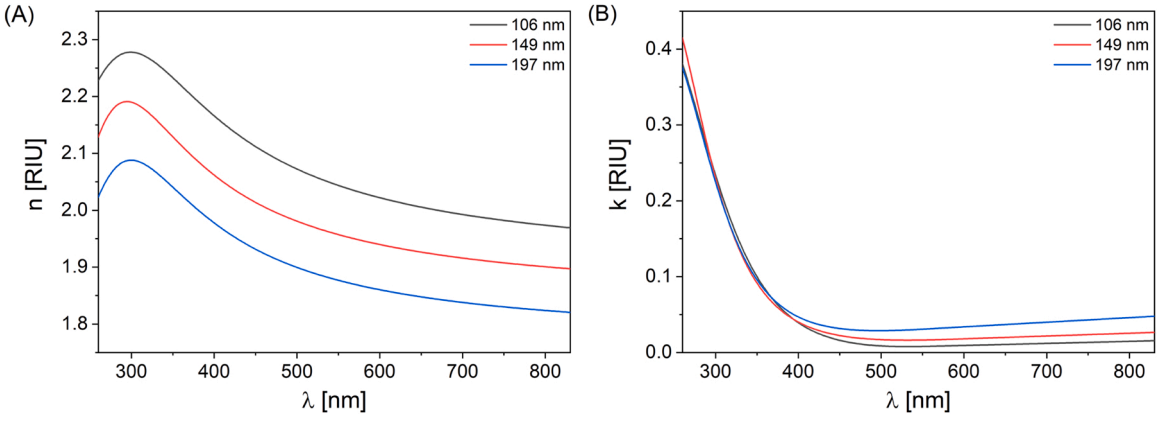

Fig. 1. Refractive index (A) and extinction coefficient (B) of different in thickness FTO films deposited on the reference silicon wafers.

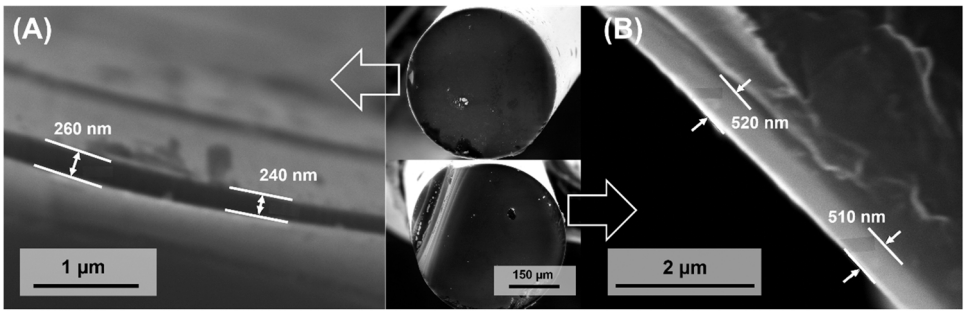

Fig. 2. The SEM images of FTO thin films deposited on the optical fiber for two depositions, where the deposition time of the first process (A) was doubled in comparison to the second one (B).

deposition rates might be explained by relatively high pressure (5 Pa) during the deposition. At higher pressure, a large amount of gas particles in the deposition chamber occurs. An increased number of particles is followed by elastic collisions with the sputtered particles on their path from the FTO target to the substrate. Hence, the enhanced pressure results in the thermalization of sputtered target atoms and also encourages the diffusion processes [58]. The particle diffusion enables the deposition on surfaces that are not facing directly the target, i.e. on the back side of the substrate. This effect is more pronounced in the case of thin substrates, such as optical fibers. Moreover, it can contribute not only to different deposition rates but also to differences in other properties received on flat substrates and fibers. The particles deposited from behind arrive at the surface with a different energy than those deposited directly from the front.

3.2. Numerical estimation of FTO thickness for the LMR sensors

To tune FTO deposition conditions for the LMR observation in the Vis spectral range, numerical analysis of the sensing structure response was performed. The analysis was based on the model presented in [59]. In short, it relies on the transfer matrix method and assumes uniform and isotropic layers (core, thin film, and the surroundings). The experimental data, i.e., n and k measured on the reference silicon samples for the thickest film (197 nm), was used for the numerical analysis (Fig. 2; blue curves). The spectra were calculated for a wide range of coating thicknesses (from 0 to 1500 nm) forming spectral maps showing the evolution of the LMRs with the FTO film thickness (Fig. 3). Keeping in mind the deposition kinetics identified in Section 3.1, this analysis allows the deposition time to be adjusted to the spectral range of the interrogation systems. It must be noted that the simulations neglect changes of n and k with the film thickness what may have an impact on the LMR. The 1st LMR can be observed in the spectral range of the used spectrometer when the thickness of FTO does not exceed 100 nm. However, there is a narrow range of FTO thicknesses where the 1st LMR can introduce high attenuation to the monitored spectrum. A deep LMR can be achieved only at a wavelength of above 600 nm when the thickness of deposited FTO is precisely adjusted. A slight increase of FTO thickness triggers a significant redshift of the LMR and its tracking is limited due to operational range of interrogation system. For higher-order LMRs (received for the thicker films), the redshift with thickness development loses its dynamic. Also the LMRs becomes well-pronounced as lower order LMRs offer higher full width at half maximum. Fig. 3 also shows simulated spectra for two arbitrarily chosen FTO thicknesses, i.e., 250 and 500 nm. In the case of the thinner film and

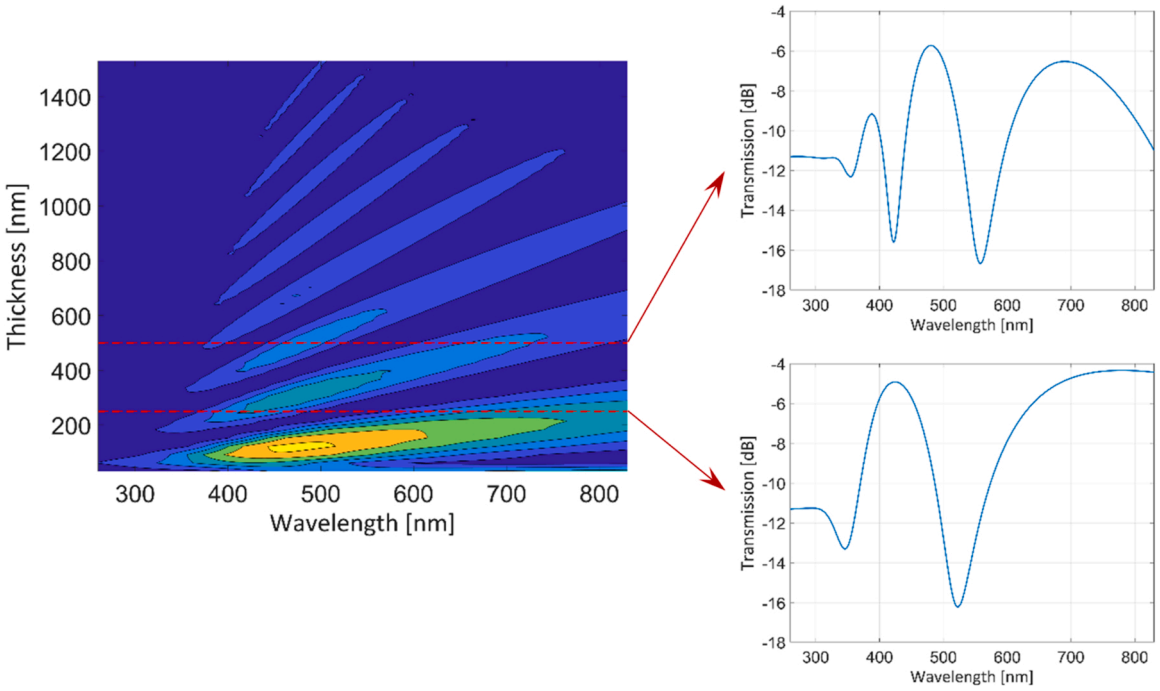

Fig. 3. Simulation of LMRs evolution for the FTO-coated optical fiber when surrounded by RI of deionized water. The darker areas between the paler once signify higher attenuation bands and the LMR appearance. The dashed lines indicate map section at the thickness reaching 500 nm (right-top) and 250 nm (right bottom).

the Vis-NIR spectral range, two LMRs can be observed. The 2nd order LMR (according to simulation, 1st order is outside the observed range) appears at c.a. $\lambda = 510$ nm and it's deeper in comparison to the 3rd order at. c.a. $\lambda = 340$ nm. When the FTO coating thickness is doubled, the 2nd order of LMR moves to the NIR, but 3rd order become well-pronounced at c.a. $\lambda = 560$ nm. The evolution of 4th and 5th order LMRs is observable for this case at the lower end of the Vis range. However, when monitoring of samples with the different film thicknesses in the same spectral range is considered, an increase in the LMR order leads to a decrease in the RI sensitivity [37]. Despite the possibility of obtaining multiple, still well-pronounced LMRs in the Vis spectrum when the thickness is higher, the RI sensitivity should be taken into consideration primarily since it has an impact on label-free biosensing applications of the device. Thus, the RI sensitivity will be discussed for experimental results shown in Section 3.3.

3.3. Impact of the FTO thickness on RI sensitivity of the LMR sensor

Based on the expected properties of FTO identified numerically as shown in Section 3.2 and their correlation with deposition parameters reported in Section 3.1, the depositions on the optical fiber sensors were performed. Bearing in mind that a well-pronounced 1st order LMR are relatively difficult to reach in the Vis spectrum, the thickness of FTO thin film was adjusted to obtain the 2nd order LMR. Also, for the 1st order undesirable separation between LMRs triggered by TE and TM modes can be more easily noticeable in the Vis spectrum [60], what favors 2nd order LMR observation for sensing purposes. In Fig. 4(A) the evolution of LMRs with the selected thicknesses is presented for the sensors immersed in a deionized water. The thickness of FTO thin film was estimated based on deposition time and the SEM images presented in Fig. 2. For the FTO thicknesses of 155 and 220 nm, only a single LMR (2nd order) can be monitored in the Vis spectral range. For the sample with 250-nm-thick FTO, the consecutive LMR becomes observable, what confirms the results of simulations. Next, the spectra of FTO-coated fibers were also measured in different n_{ext}. The LMR shift is presented in Fig. 4(B). According to these results, the sensitivity within the same order of LMR increases with thickness and reaches 220, 242 and 278 nm/RIU in a range of $n_{ext} = 1.333–1.415$ RIU for samples with 155-, 220-, and 250-nm-thick films, respectively. For the 3rd order LMR, the RI sensitivity is significantly lower than for the 2nd order and reaches only 87 nm/RIU. With increasing FTO thickness, the RI sensitivity for the 3rd order increases as well [37]. However, it does not reach the value as for the 2nd order in the examined wavelength range. It must be noted that the RI sensitivity received here for the 2nd order LMR is comparable to those achieved for other LMR sensors investigated in the Vis-NIR region and coated with ITO [61] or ZrO_2 [36]. Hence, FTO can be used as a lossy mode guiding material to the same extent as the previously reported thin films.

Since the thickness may have an impact on electrical and EC properties, the same deposition procedure was repeated but deposited FTO films were significantly thicker than for samples shown in Fig. 4. The results were presented in Fig. S1 in Supplementary Information and confirm lower RI sensitivity for the higher order's LMR, what agrees with findings reported previously in [37].

3.4. Reflective configuration of the FTO-LMR sensors

This section presents the possibility of developing FTO-LMR sensors also in the reflective configuration. The comparison between spectra received for the transmissive and reflective variants of the sensors and their evolution with n_{ext} is presented in Fig. 5. For these sensors, the FTO coatings were deposited at the same conditions as for the sample shown in Fig. 2(A). A high agreement of optical responses between the two variants of the sensors is achieved. The RI sensitivity was also comparable and reached 433 nm/RIU and 449 nm/RIU in a range of $n_{ext} = 1.333–1.418$ RIU for the transmissive and reflective configuration, respectively. The measured RI sensitivity was higher in comparison to the sensors analyzed in the previous section and indicated a higher n of FTO coating received in this deposition configuration. It must be noted that in this set of depositions the samples were placed further from the sputtered target than for those reported in Section 3.3. Increase of the distance has made the deposition rate lower. A similar effect of target-substrate distance was also observed in the case of ITO films [62]. The effect is attributed to different energy flux to the substrate which influences the growth of the film with a different fraction of crystalline phase in an amorphous film matrix [47,63]. The same mechanism is expected also for FTO. The results for the sensor in the reflective configuration presented previously in Fig. 2(B) are shown in Supplementary Information (Fig. S2), where the RI sensitivity is also reported. Importantly, both the presented configurations can be applied to the same extent after adjusting deposition parameters.

3.5. EC performance of the FTO-LMR sensors

The FTO samples in the reflective configuration were finally investigated as working electrodes in the EC setup. Fig. 6(A) presents CV results for the sample where FTO thickness reaches 250 nm (Fig. 2(A) – the same as those discussed in Section 3.4). The CVs were recorded at scan rates of 10 and 100 mV/s using 1 mM 1,1′-Ferrocenedimethanol (RedOx couple) in 0.01 M PBS and pristine 0.01 M PBS as the reference. As a result of E sweeping at the FTO electrode, the changes in the current show no typical RedOx peaks resulting from oxidation and reduction reactions of the RedOx probe. The hysteresis in the current while E sweeping is attributed to capacitive currents originating from the

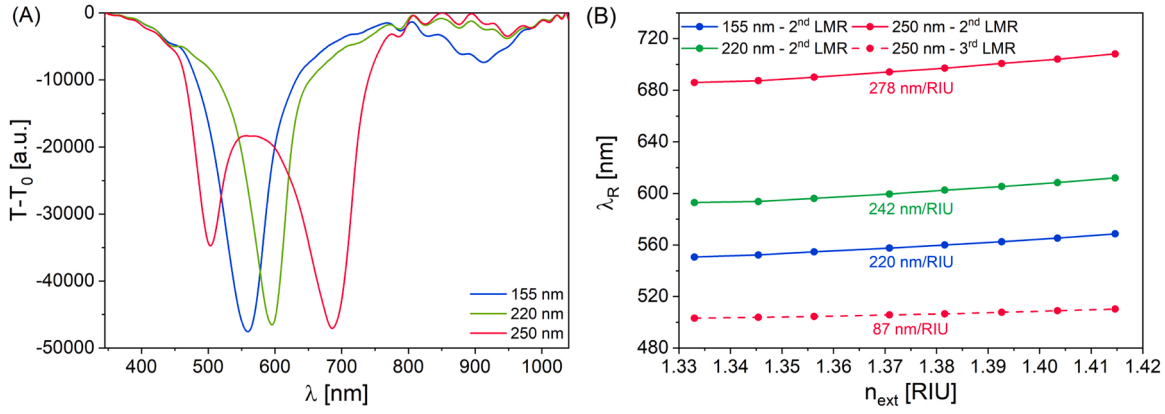

Fig. 4. Optical spectra of FTO-LMR sensors with the coating thicknesses of 155, 220 and 250 nm acquired in deionized water (A) and corresponding LMR wavelength (λ_R) evolution with n_{ext} (B). The thickness of FTO thin film was estimated based on deposition time and the SEM images presented in Fig. 2.

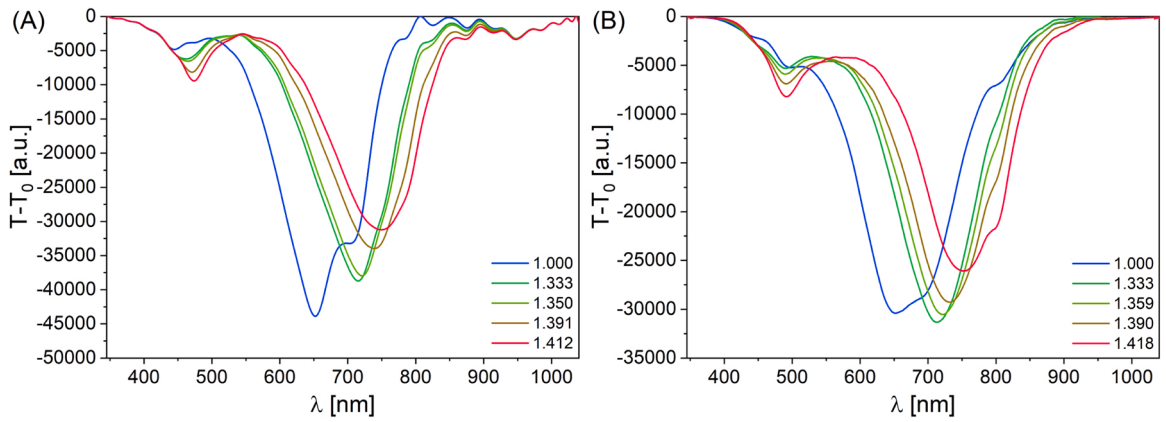

Fig. 5. Evolution of optical spectra for transmissive (A) and reflective (B) FTO-LMR sensors with n_{ext} for the FTO coating thickness reaching 250 nm.

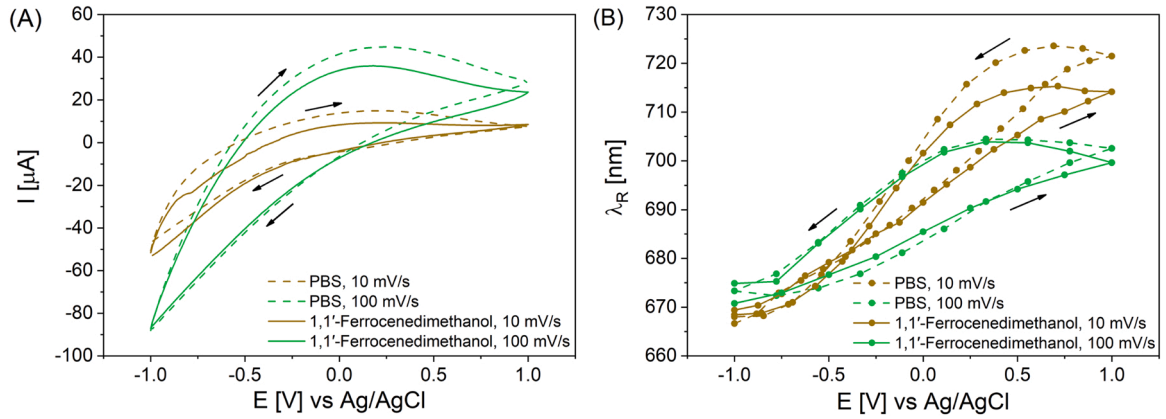

Fig. 6. (A) EC response of the 250-nm-thick reflective FTO-LMR sensor during E scanning in PBS and 1,1′-Ferrocenedimethanol with scan rates of 10 mV/s and 100 mV/s. (B) Corresponding λ_R simultaneously registered during the EC process. The arrows indicate E scanning direction.

charging and discharging of the electrical double-layer in the closest vicinity of the FTO surface. For this FTO thickness, the Faraday currents related to charge transfer induced by RedOx processes were not observed. These results imply that electron transfer between the electrode and the electrolyte was suppressed, particularly in the presence of the RedOx couple. Electron transfer was also suppressed at higher scan rates (100 mV/s) when the size of the diffusion layer is minimized. Slightly higher capacitive currents were observed for faster scan rates and are attributed to the enhanced charge depletion at the FTO-electrolyte interface. Nevertheless, no typical Faradic currents were recorded allowing for EC sensing applications of the device [64]. The optical response of the sensor recorded simultaneously with E sweeping (Fig. 6(B)) reveals the significant variation in the λ_R with the applied E. The λ_R shift in the E range − 1–1 V exceeds 55 nm for PBS at a scan rate of 10 mV/s. For 100 mV/s the λ_R shift is lower and in the same E range reaches 32 nm, which is contrary to the current recorded during CV for those two cases. The main factor influencing the λ_R, in this case, is the RI of the FTO. By applying E to the FTO-electrode the carrier concentration in the semiconductor changes what is followed by its RI [61]. The hysteresis effect observed in optical readout (Fig. 6(B)) also depends strongly on the capacitive currents, thus, it could be ascribed to an electrical double-layer formed at the FTO surface during E cycling. The changes are the most significant in the space-charge layer of FTO film at the interface between the electrode and the electrolyte, where the carrier forms an accumulation and depletion layer. From optical point of view changes in distribution of the charge carriers correspond to optical properties of the material [65]. The factors such as adsorption of the RedOx couple molecules or formation of accumulation layer (i.e. ions, electrons) at electrode/electrolyte interface contribute particularly to hysteresis slope and shape. Generally, depletion layer formation does not influence much the RI of a semiconductor [64], thus it should not affect the λ_R. Such an effect has been observed in the work devoted to ITO-LMR device, i.e., when positive E was applied to the electrode the λ_R shift was inhibited [65]. Different responses than typically for the ITO-LMR device can be observed in Fig. 6(B). In both PBS electrolytes with and without RedOx couple during positive sweep from − 1–1 V the shift is significant in the negative as well as in the positive E range. This effect is even more noticeable for a scan rate of 10 mV/s where majority charge carriers (electrons in case of FTO) have more time to transfer in the material and form accumulation layer at the FTO electrode/electrolyte interface. Additionally, when the RedOx couple is present, the λ_R shift in positive E range is slightly less distinctive than for PBS. This could be caused by adsorption of the RedOx couple molecules on the FTO. Although ferrocene derivatives are normally considered as an outer sphere RedOx couple, there are clear indications that they can adsorb on a variety of carbon electrode surfaces [66–69], as well as on noble-metal electrodes [70]. Ferrocenes have also been adsorbed on silica for spectroscopic studies [71]. The effect might be exacerbated by the relatively high ratio of ferrocene to supporting electrolyte.

Analyzing the simplified band diagram of n-type semiconductor/electrolyte with the RedOx couple (Fig. 7(A)), the λ_R shift for considered FTO-based electrode in whole E range is possible when the standard E of the RedOx couple (E_{REDOX}) is located in the conduction band of semiconductor before contact with the electrolyte. After the contact, bending of conductive band edge takes place due to accumulating electrons at the interface [72]. Nevertheless, this fact contradicts with CV observations

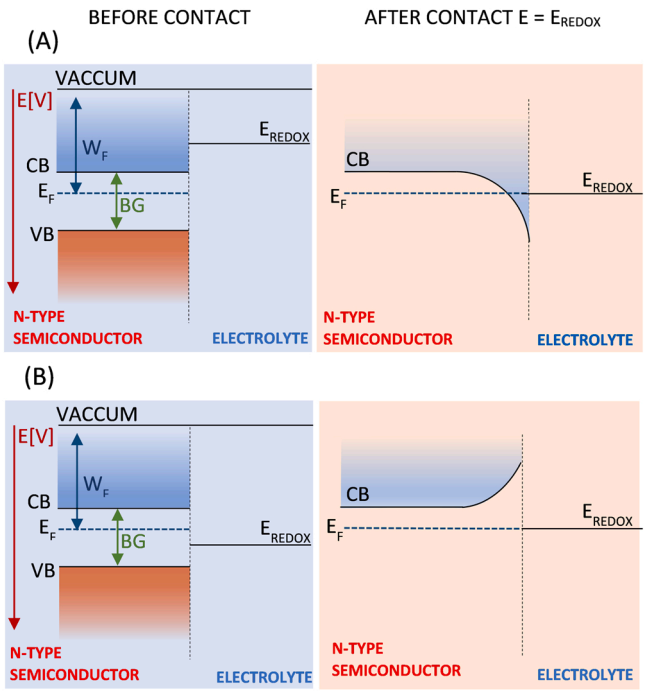

Fig. 7. The proposed bandgap diagram of FTO electrode before and after contact with an electrolyte containing RedOx couple. The standard RedOx couple potentials (E_{REDOX}) are considered to be located in the conduction band (A) or in the bandgap (B) of semiconductor. The applied E influence the carrier concentration in space-charge layer what is presented as a bending of conduction band edge. CB: conduction band, VB: valence band, E_F: Fermi level energy, WF: work function, BG: bandgap.

shown in Fig. 6(A), which are far from the typical reversible electrodes revealing rather diffusion-limited charge transfer. Such EC character is usually observed for n-type semiconductors once the standard potential of the RedOx couple is located in the bandgap (Fig. 7(B)). Once the negative E is applied, the band bending is depressed, while the electrode stays in a depletion mode and the concentration of electrons at the interfaces is low. Thus, the optical effect ought to be here driven by other factors i.e. chloride ions production [73] or phosphates oxidation. The other possible reason may be the relatively high resistivity of the deposited FTO coatings. In particular, the transparent conductive oxides (TCOs) are polycrystalline materials with structural defects [74] increasing resistivity by charge scattering.

To improve EC performance of the sensors, thicker FTO films were investigated next. Longer deposition results in higher thickness, especially with thermal treatment, what could improve crystallinity and consequently the conductivity of the films [53,74,75]. It was already reported that the longer deposition of FTO reduces its resistivity [76,77]. Thus, we have fabricated the FTO-LMR sensor in the reflective configuration, where the FTO coating thickness was doubled (approx. 500 nm) in comparison to the sensor for which the results were shown in Fig. 6. The detailed analysis of the optical performance of the device with 500-nm-thick FTO and the influence of the FTO thickness on the RI sensitivity was shown in Supplementary Information. The CV curves obtained for the sample with thicker FTO are shown in Fig. 8(A). Those curves as for the thinner FTO exhibit capacitive currents originating from diffusion layer for bare PBS electrolyte, but also reversible electron transfer at the electrode/electrolyte interface (Faradaic current) of the 1, 1′-Ferrocenedimethanol RedOx couple.

The estimated peak-to-peak separation, defined as E difference between reduction and oxidation peaks (ΔE_P), which describes the electron transfer kinetics, reaches 230 mV. This value is comparable with the results revealed for analogous LMR structure coated with ITO [27]. In this case, electrons from the reduced form of the RedOx couple are accumulated in conduction band (CB) allowing for further oxidation processes of the RedOx couple (Fig. 7(A)). Thus, the FTO behaves here as a reversible metallic electrode. Moreover, for the thicker FTO coating the E-induced λ_R modulation reveals slightly boosted. In the positive E range the λ_R shift during positive sweep reaches 30 nm in PBS analogously for thinner FTO coating, but for lower scan rates (20 vs 10 mV/s) (Fig. 8(B)). These results are substantial because in the previous works dedicated to ITO-LMR electrode, the appearance of RedOx current peaks simultaneously with λ_R shift has been hardly achieved [27,78]. When deposition parameters for ITO were tuned to reduce resistivity and obtain RedOx current peaks in the CV, bandgap also changes its location and accumulation layer has not been developed to the same extent as for FTO. These results confirm that despite similar optical parameters (n and k) of FTO and ITO, their bandgaps are considerably different. Apparently, the observed effect can be explained by different energy band structure of these films. The FTO electrodes revealed the n-type conductivity at low anodic potentials with tuned band gap and surprisingly p-type at high anodic potentials thanks to the formation of the degenerated SnO-like surface layer throughout the oxygen evolution reaction [44]. Furthermore, the FTO coating can be considered not only as a plain current collector or electrode, but also as a highly efficient photoelectrochemical and photoelectrocatalytic surface [73] inducing photogeneration of highly separated charge carriers and oxidizing species (i.e. chlorides and hydroxyls) under illumination [79].

Complex nature of FTO character should be taken into account during design a dual-domain sensor for a specific sensing application. In the concept where one domain confirms the results obtained in the second one, the changes in optical response induced by E sweeping in

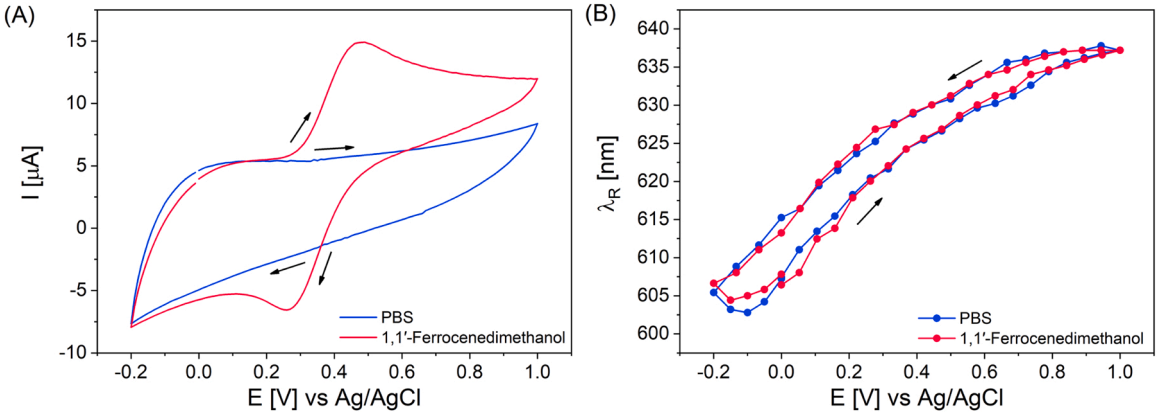

Fig. 8. (A) EC response of the 500-nm-thick reflective FTO-LMR sensor during E scanning in PBS and 1,1′-Ferrocenedimethanol with a scan rate of 20 mV/s. (B) Corresponding λ_R simultaneously registered during the EC process. The arrows indicate E scanning direction.

whole E range is desirable. Biosensing is a suitable example where typically reduction of electric current flow and accumulation layer thickness induced by biofilm binding are more noticeable than RI changes induced by the same factor.

3.6. Dual-domain label-free biosensing with FTO-LMR sensor

The performance of the discussed above dual-domain FTO-LMR sensor for label-free biosensing is discussed in this section. Biotin and streptavidin were applied as receptor and target material, respectively, due to their strong binding and thus capability to verify label-free biosensing properties of the FTO-LMR approach. For the purpose of this part of the experiment a batch of samples in reflective configuration with an FTO thickness of c.a. 1 μm was prepared. Relatively high FTO thickness has been chosen due to partly improved sensor performance for this range of FTO thickness, i.e. well-visible RedOx current peaks and stronger E-induced λ_R modulation, but lower RI sensitivity. Optical response of the obtained sensors is comparable to the one shown in Fig. S1(A). The CV curves shown in Fig. 9 measured before functionalization indicate ΔE_P reaching only 140 mV. Lower ΔE_P, i.e. better EC performance of the sensor with increase in FTO thicknesses stay in agreement with findings reported in Section 3.5. In the optical domain in turn, the λ_R shift is suppressed when compared to sensors with lower FTO thickness and in positive E range it reaches 17 nm (Fig. 10(A)). According to discussions reported in Section 3.5, for higher FTO thickness more electrons participate in RedOx process and formation of the accumulation layer with applied E is not as effective as for thinner FTO films.

The readouts received in EC and optical domains, as well as cross-domain interactions during the label-free biosensing experiment are discussed next. In the EC domain, every step of FTO-LMR sensor modification leads to decrease and increase in RedOx peaks current and ΔE_P, respectively (Fig. 9). The effect corresponds to blocking the active surface of the FTO when chemical compound and biological species bind. According to the ΔE_P changes, the electrode surface was blocked the most after exposure to APTES. Silanization process has created an even, but thin layer, which thoroughly reduced the active sensor's surface. Binding of biotin that followed the functionalization process resulted in ΔE_P increase by only 4 mV. Relatively low response can be attributed to sub nanometer size of the molecule and therefore its limited ability to reducing the active surface of the working electrode. After incubation in BSA aiming to prevent against unspecific binding of streptavidin further ΔE_P increase with streptavidin concentration has also been achieved. Considering the molecular dimensions of streptavidin (4.2 nm × 4.2 nm × 5.6 nm) [80], even the smallest concentration of it should additionally prevent from charge transfer with the RedOx probe [81]. The most significant increase in ΔE_P has been observed for the highest applied streptavidin concentration.

In the optical domain changes taking place on the sensor surface correspond to the λ_R shift. Consecutive experimental steps concerning introduction of streptavidin results in general λ_R shift towards longer wavelengths (Fig. 10(B)). It is caused by RI increase in the vicinity of the FTO surface induced by binding of the biological material. However, RI-induced λ_R shift for $E = 0$ V is relatively low (Fig. 10(A)). Some more information can be obtained from cross-domain interactions, i.e. when E is applied (Fig. 10). Materials gathered on the FTO active surface have an impact on formation of charge carrier distribution in the FTO close to its surface and change optical properties of the material. Thus, observations of presence of the biological layer are significantly influenced by applied E. It can be seen that the λ_R shift after each step of the biosensing procedure is clearly observed when the E is applied. The results obtained for $E = -0.2$ V agree well with those obtained in EC domain and shown in Fig. 9(B). In contrast, when $E = 1$ V the λ_R shift obtained for low streptavidin concentrations is well observed. As a binding of biological material influences the RI on the surface only slightly, dual-domain approaches can significantly improve the sensing capability of the device.

4. Conclusions

In this work, we have demonstrated the optical and electrochemical response of the FTO-coated lossy-mode resonance (LMR) sensor. For this type of dual-domain sensors, ITO was mainly investigated so far, thus we have considered FTO as an alternative. Optical properties of FTO deposited by magnetron sputtering show distinct tendency with deposition time, i.e., its n decreasing while k increasing slightly, but most importantly FTO's optical properties allows for guiding lossy modes. Experimentally obtained optical properties of FTO make possible simulation of sensor response in the optical domain, identification of the suitable film thickness and fabrication of a series of FTO-LMR sensor accordingly. The influence of FTO coating thickness on LMR development and RI sensitivity of the FTO-LMR device was experimentally confirmed. Comparing to the previously used TCOs able to guide lossy modes, especially ITO, the FTO-LMR sensors show similar RI sensitivity in the Vis spectral range, i.e., up to 450 nm/RIU in the range n_{ext} = 1.33–1.40 RIU. Furthermore, we have shown a reflective configuration of the LMR sensor which facilitate a probe-like application. According to the results, the reflective configuration offers similar properties, including RI sensitivity, as for transmissive counterpart, but enhances functionality of the approach. We believe that the RI sensitivity can be further enhanced when the optimized FTO is deposited on some advanced optical fiber sensing device.

The response of the reflective FTO-LMR sensors in electrochemical domain was considered next. As resistivity is one of key parameters for

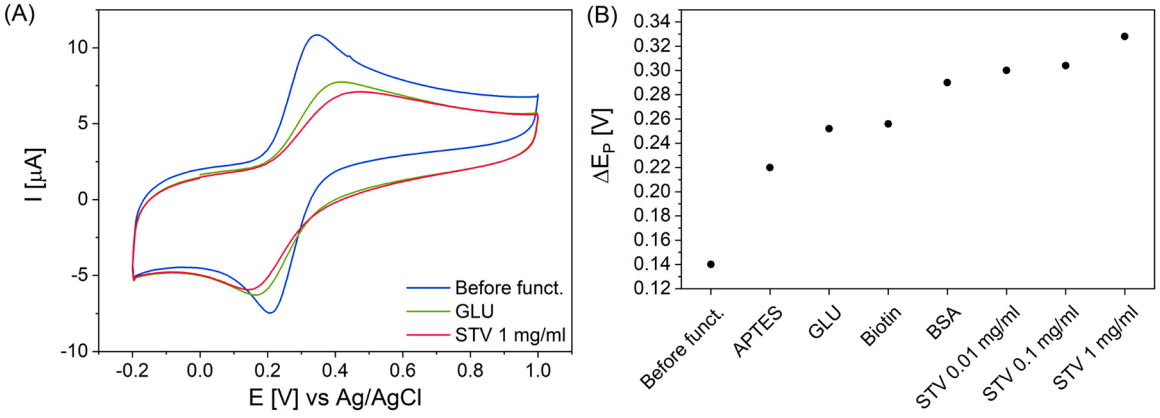

Fig. 9. (A) EC response of 1-μm-thick reflective FTO-LMR sensor during E scanning in 1,1′-Ferrocenedimethanol with a scan rate of 20 mV/s after selected steps towards streptavidin (STV) detection. (B) Corresponding increase of ΔE_P after consecutive steps of the biosensing experiment.

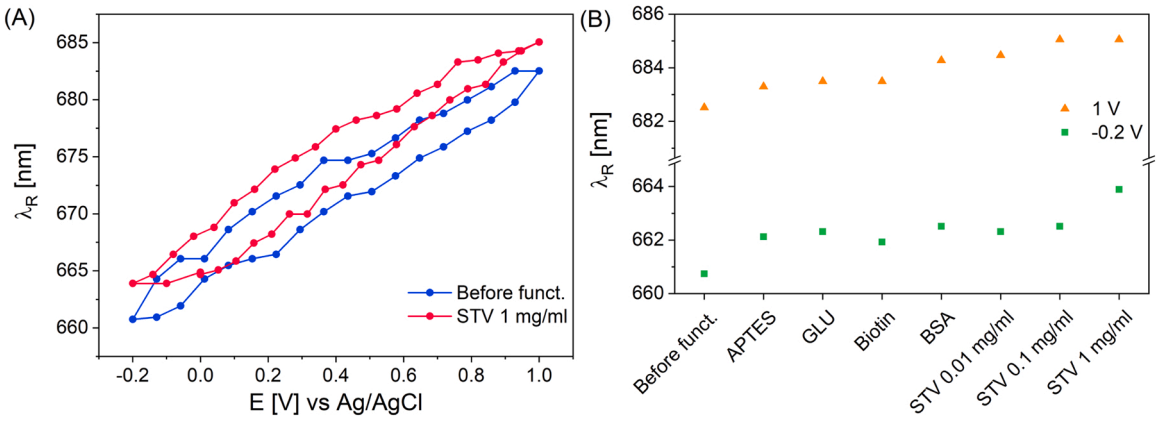

Fig. 10. (A) λ_R measured during the EC process after selected steps of biosensing procedure. (B) λ_R shift after consecutive steps of the procedure for different *E* applied.

working electrode, the effective electrochemical response in the presence of RedOx couple was received for thick, c.a. 500 nm, FTO film. Electrochemical performance of the FTO-LMR device is comparable to ITO-LMR alternatives. However, the effect of applied potential sweeping on the optical response was the most important observation. We reveal that electronic band structure of semiconductor electrode such as FTO is crucial for opto-electrochemical dual-domain sensor performance. The FTO-LMR electrode, in contrast to ITO-LMR electrode, is vulnerable for potential sweeping even when RedOx reactions occur. These phenomena are originated by accumulation layer developed at the interface between electrode and electrolyte what has an impact on optical properties of the FTO. Accumulation layer of such an extent has not been developed in the case of the ITO-LMR electrode and the applied RedOx couple due to different electronic bandgap structure of ITO. Thus, to adjust lossy mode guiding and at the same time electrochemical response it is required to precisely optimize FTO properties at the stage of the thin film deposition. Finally, the designed FTO-LMR dual-domain sensor was successfully applied for label-free biosensing using biotin and streptavidin as receptor and target material, respectively. The binding of the target material has been observed in both electrochemical and optical domains, as well as in a cross-domain response. While the results in both the domains cross-verify each other, cross-domain interactions can be used for enhancing sensing capabilities. Results reported in this paper for FTO can be considered as an introduction to a wide spectrum of dual-domain FTO applications based on various optical and electrochemical sensing configurations.

CRediT authorship contribution statement

D. Burnat: Investigation, Data curation, Writing – original draft, Writing – review & editing, **P. Sezemsky:** Investigation, Data curation, Writing – original draft, **K. Lechowicz:** Investigation, Visualization, **M. Koba:** Methodology, Formal analysis, Data curation, Writing – original draft, Writing – review & editing, **M. Janczuk-Richter:** Investigation, Data curation, **M. Janik:** Methodology, Formal analysis, Writing – original draft, Writing – review & editing, **V. Stranak:** Funding acquisition, Project administration, Conceptualization, Methodology, Formal analysis, Supervision, Resources, Writing – original draft, **J. Niedziółka-Jönsson:** Formal analysis, Supervision, Writing – original draft, Writing – review & editing, **R. Bogdanowicz:** Formal analysis, Writing – original draft, Writing – review & editing, **M. Śmietana:** Funding acquisition, Project administration, Conceptualization, Methodology, Formal analysis, Supervision, Resources, Writing – original draft, Writing – review & editing.

Declaration of Competing Interest

The authors declare that they have no known competing financial interests or personal relationships that could have appeared to influence the work reported in this paper.

Acknowledgments

Research was funded by CB POB Materials Technologies of Warsaw University of Technology within the Excellence Initiative: Research University (IDUB) program and by the National Science Centre (NCN), Poland, OPUS program, project No. 2019/35/B/ST7/04388. Financial support of project No. 19-20168S by Czech Science Foundation agency (GACR) is also acknowledged. The international collaboration was encouraged by a bilateral Mobility project 8JPL19012 from MSMT Czech Republic and grant No. PPN/BIL/2018/1/00126 from the National Agency for Academic Exchange (NAWA), Poland. M. Janik acknowledges the support from the Foundation for Polish Science within the START 2021 program. Support received from Dr. Martin Jönsson-Niedziółka within discussion of electrochemical results and from Olga Zatorska and Ewa Roźniecka within biosensing experiments is also acknowledged.

Appendix A. Supporting information

Supplementary data associated with this article can be found in the online version at doi:10.1016/j.snb.2022.132145.

References

[1] X. Huang, D. Xu, J. Chen, J. Liu, Y. Li, J. Song, X. Ma, J. Guo, Smartphone-based analytical biosensors, Analyst 143 (2018) 5339–5351, https://doi.org/10.1039/c8an01269e.
[2] S. Gupta, C.N. Murthy, C.R. Prabha, Recent advances in carbon nanotube based electrochemical biosensors, Int. J. Biol. Macromol. 108 (2018) 687–703, https://doi.org/10.1016/j.ijbiomac.2017.12.038.
[3] X. Wang, M. Que, M. Chen, X. Han, X. Li, C. Pan, Z.L. Wang, Full dynamic-range pressure sensor matrix based on optical and electrical dual-mode sensing, Adv. Mater. 29 (2017) 1605817, https://doi.org/10.1002/adma.201605817.
[4] Q. Jing, G. Zhu, W. Wu, P. Bai, Y. Xie, R.P.S. Han, Z.L. Wang, Self-powered triboelectric velocity sensor for dual-mode sensing of rectified linear and rotary motions, Nano Energy 10 (2014) 305–312, https://doi.org/10.1016/j.nanoen.2014.09.018.
[5] M. Śmietana, M. Koba, P. Sezemsky, K. Szot-Karpińska, D. Burnat, V. Stranak, J. Niedziółka-Jönsson, R. Bogdanowicz, Simultaneous optical and electrochemical label-free biosensing with ITO-coated lossy-mode resonance sensor, Biosens. Bioelectron. 154 (2020), 112050, https://doi.org/10.1016/j.bios.2020.112050.
[6] J. Juan-Colás, Dual-Mode Electro-photonic Silicon Biosensors, first ed., Springer, Cham, 2017 https://doi.org/10.1007/978-3-319-60501-2.
[7] F. Chiavaioli, A. Giannetti, S. Tombelli, C. Trono, I. Del Villar, I.R. Matias, P. Zubiate, C.R. Zamarreño, F.J. Arregui, F. Baldini, Lossy Mode Resonance Enabling Ultra-Low Detection Limit for Fibre-Optic Biosensors, in: Sensors Microsystems,

Proc. 20th AISEM 2019 Natl. Conf., Springer, 2020: pp. 321–327. https://doi.org/10.1007/978–3-030–37558-4_49.
[8] F. Esposito, L. Sansone, A. Srivastava, F. Baldini, S. Campopiano, F. Chiavaioli, M. Giordano, A. Giannetti, A. Iadicicco, Long period grating in double cladding fiber coated with graphene oxide as high-performance optical platform for biosensing, Biosens. Bioelectron. 172 (2021), 112747, https://doi.org/10.1016/J.BIOS.2020.112747.
[9] F. Chiavaioli, P. Zubiate, I. Del Villar, C.R. Zamarreño, A. Giannetti, S. Tombelli, C. Trono, F.J. Arregui, I.R. Matias, F. Baldini, Femtomolar detection by nanocoated fiber label-free biosensors, ACS Sens. 3 (2018) 936–943, https://doi.org/10.1021/ACSSENSORS.7B00918.
[10] G. Moro, F. Chiavaioli, S. Liberi, P. Zubiate, I. Del Villar, A. Angelini, K. De Wael, F. Baldini, L.M. Moretto, A. Giannetti, Nanocoated fiber label-free biosensing for perfluorooctanoic acid detection by lossy mode resonance, Results Opt. 5 (2021), 100123, https://doi.org/10.1016/J.RIO.2021.100123.
[11] B. Shao, Z. Xiao, Recent achievements in exosomal biomarkers detection by nanomaterials-based optical biosensors - a review, Anal. Chim. Acta 1114 (2020) 74–84, https://doi.org/10.1016/J.ACA.2020.02.041.
[12] H. Du, Z. Li, Y. Wang, Q. Yang, W. Wu, Nanomaterial-based optical biosensors for the detection of foodborne bacteria, Food Rev. Int. (2020) 1–30, https://doi.org/10.1080/87559129.2020.1740733.
[13] V. Garzón, D.G. Pinacho, R.-H. Bustos, G. Garzón, S. Bustamante, Optical biosensors for therapeutic drug monitoring, Biosensors 9 (2019) 132, https://doi.org/10.3390/BIOS9040132.
[14] V.C. Diculescu, A.M. Chiorcea-Paquim, A.M. Oliveira-Brett, Applications of a DNA-electrochemical biosensor, TrAC Trends Anal. Chem. 79 (2016) 23–36, https://doi.org/10.1016/j.trac.2016.01.019.
[15] A. Pereira, M. Sales, L. Rodrigues, Biosensors for rapid detection of breast cancer biomarkers, in: Advanced Biosensors for Health Care Applications, Elsevier, 2019, pp. 71–103, https://doi.org/10.1016/b978-0-12-815743-5.00003-2.
[16] M.B. Akolpoglu, U. Bozuyuk, P. Erkoc, S. Kizilel, Biosensing–drug delivery systems for in vivo applications, in: Advanced Biosensors for Health Care Applications, Elsevier, 2019, pp. 249–262, https://doi.org/10.1016/b978-0-12-815743-5.00009-3.
[17] U. Anik, Electrochemical medical biosensors for POC applications, in: Medical Biosensors for Point of Care Applications, Elsevier Inc, 2017, pp. 275–292, https://doi.org/10.1016/B978-0-08-100072-4.00012-5.
[18] M. Śmietana, M. Sobaszek, B. Michalak, P. Niedziałkowski, W. Białobrzeska, M. Koba, P. Sezemsky, V. Stranak, J. Karczewski, T. Ossowski, R. Bogdanowicz, Optical monitoring of electrochemical processes with ITO-based lossy-mode resonance optical fiber sensor applied as an electrode, J. Light. Technol. 36 (2018) 954–960, https://doi.org/10.1109/JLT.2018.2797083.
[19] A. Blidar, B. Feier, M. Tertis, R. Galatus, C. Cristea, Electrochemical surface plasmon resonance (EC-SPR) aptasensor for ampicillin detection, Anal. Bioanal. Chem. 411 (2019) 1053–1065, https://doi.org/10.1007/s00216-018-1533-5.
[20] W. Putzbach, N. Ronkainen, Immobilization techniques in the fabrication of nanomaterial-based electrochemical biosensors: a review, Sensors 13 (2013) 4811–4840, https://doi.org/10.3390/s130404811.
[21] D. Burnat, M. Janczuk-Richter, P. Niedziałkowski, W. Białobrzeska, P. Sezemsky, M. Koba, V. Stranak, R. Bogdanowicz, T. Ossowski, J. Niedziółka-Jönsson, M. Smietana, Optical fiber lossy-mode resonance sensors with doped tin oxides for optical working electrode monitoring in electrochemical systems, in: Proc. SPIE - Int. Soc. Opt. Eng., 2019: p. 111991 O. https://doi.org/10.1117/12.2541354.
[22] J. Juan-Colás, A. Parkin, K.E. Dunn, M.G. Scullion, T.F. Krauss, S.D. Johnson, The electrophotonic silicon biosensor, Nat. Commun. 7 (2016) 1–7, https://doi.org/10.1038/ncomms12769.
[23] J.P. Bearinger, J. Vörös, J.A. Hubbell, M. Textor, Electrochemical optical waveguide lightmode spectroscopy (EC-OWLS): A pilot study using evanescent-field optical sensing under voltage control to monitor polycationic polymer adsorption onto indium tin oxide (ITO)-coated waveguide chips, Biotechnol. Bioeng. 82 (2003) 465–473, https://doi.org/10.1002/BIT.10591.
[24] Y. Yuan, T. Guo, X. Qiu, J. Tang, Y. Huang, L. Zhuang, S. Zhou, Z. Li, B.-O. Guan, X. Zhang, J. Albert, Electrochemical surface plasmon resonance fiber-optic sensor: in situ detection of electroactive biofilms, Anal. Chem. 88 (2016) 7609–7616, https://doi.org/10.1021/ACS.ANALCHEM.6B01314.
[25] Y. Si, J. Lao, X. Zhang, Y. Liu, S. Cai, A. Gonzalez-Vila, K. Li, Y. Huang, Y. Yuan, C. Caucheteur, T. Guo, Electrochemical plasmonic fiber-optic sensors for ultra-sensitive heavy metal detection, J. Light. Technol. 37 (2019) 3495–3502, https://doi.org/10.1109/JLT.2019.2917329.
[26] J. Lao, P. Sun, F. Liu, X. Zhang, C. Zhao, W. Mai, T. Guo, G. Xiao, J. Albert, In situ plasmonic optical fiber detection of the state of charge of supercapacitors for renewable energy storage, Light Sci. Appl. 7 (2018) 1–11, https://doi.org/10.1038/s41377-018-0040-y.
[27] P. Niedziałkowski, W. Białobrzeska, D. Burnat, P. Sezemsky, V. Stranak, H. Wulff, T. Ossowski, R. Bogdanowicz, M. Koba, M. Śmietana, Electrochemical performance of indium-tin-oxide-coated lossy-mode resonance optical fiber sensor, Sens. Actuators B Chem. 301 (2019), 127043, https://doi.org/10.1016/j.snb.2019.127043.
[28] I. Del Villar, C.R. Zamarreño, M. Hernaez, F.J. Arregui, I.R. Matias, Lossy mode resonance generation with indium-tin-oxide-coated optical fibers for sensing applications, J. Light. Technol. 28 (2010) 111–117, https://doi.org/10.1109/JLT.2009.2036580.
[29] I. Del Villar, F.J. Arregui, C.R. Zamarreño, J.M. Corres, C. Bariain, J. Goicoechea, C. Elosua, M. Hernaez, P.J. Rivero, A.B. Socorro, A. Urrutia, P. Sanchez, P. Zubiate, D. Lopez, N. De Acha, J. Ascorbe, I.R. Matias, Optical sensors based on lossy-mode resonances, Sens. Actuators B Chem. 240 (2017) 174–185, https://doi.org/10.1016/j.snb.2016.08.126.
[30] S.H. Jeong, S.H. Woo, T.H. Han, M.H. Park, H. Cho, Y.H. Kim, H. Cho, H. Kim, S. Yoo, T.W. Lee, Universal high work function flexible anode for simplified ito-free organic and perovskite light-emitting diodes with ultra-high efficiency, NPG Asia Mater. 9 (2017), https://doi.org/10.1038/am.2017.108.
[31] H. Zhou, X. Zhu, H. Li, H. Lan, Fabrication of the large-area flexible transparent heaters using electric-field-driven jet deposition micro-scale 3D printing, Adv. Opt. Technol. 8 (2019) 217–223, https://doi.org/10.1515/aot-2019-0021.
[32] J.D. Benck, B.A. Pinaud, Y. Gorlin, T.F. Jaramillo, Substrate selection for fundamental studies of electrocatalysts and photoelectrodes: inert potential windows in acidic, neutral, and basic electrolyte, PLoS One 9 (2014), e107942, https://doi.org/10.1371/journal.pone.0107942.
[33] A. Cirocka, D. Zarzeczańska, A. Wcisło, J. Ryl, R. Bogdanowicz, B. Finke, T. Ossowski, Tuning of the electrochemical properties of transparent fluorine-doped tin oxide electrodes by microwave pulsed-plasma polymerized allylamine, Electrochim. Acta 313 (2019) 432–440, https://doi.org/10.1016/j.electacta.2019.05.046.
[34] D. Burnat, M. Koba, L. Wachnicki, S. Gieraltowska, M. Godlewski, M. Śmietana, Refractive index sensitivity of optical fiber lossy-mode resonance sensors based on atomic layer deposited TiOx thin overlay, in: Proc. SPIE - Int. Soc. Opt. Eng., 2016: p. 99161 G. https://doi.org/10.1117/12.2236908.
[35] I. Del Villar, C.R. Zamarreño, P. Sanchez, M. Hernaez, C.F. Valdivielso, F. J. Arregui, I.R. Matias, Generation of lossy mode resonances by deposition of high-refractive-index coatings on uncladded multimode optical fibers, J. Opt. 12 (2010), 095503, https://doi.org/10.1088/2040-8978/12/9/095503.
[36] K. Kosiel, M. Koba, M. Masiewicz, M. Śmietana, Tailoring properties of lossy-mode resonance optical fiber sensors with atomic layer deposition technique, Opt. Laser Technol. 102 (2018) 213–221, https://doi.org/10.1016/j.optlastec.2018.01.002.
[37] I. Del Villar, M. Hernaez, C.R. Zamarreno, P. Sánchez, C. Fernández-Valdivielso, F. J. Arregui, I.R. Matias, Design rules for lossy mode resonance based sensors, Appl. Opt. 51 (2012) 4298–4307, https://doi.org/10.1364/AO.51.004298.
[38] Z. Banyamin, P. Kelly, G. West, J. Boardman, Electrical and optical properties of fluorine doped tin oxide thin films prepared by magnetron sputtering, Coatings 4 (2014) 732–746, https://doi.org/10.3390/coatings4040732.
[39] A.E. Rakhshani, Y. Makdisi, H.A. Ramazaniyan, Electronic and optical properties of fluorine-doped tin oxide films, J. Appl. Phys. 83 (1998) 1049–1057, https://doi.org/10.1063/1.366796.
[40] S. Shanthi, C. Subramanian, P. Ramasamy, Investigations on the optical properties of undoped, fluorine doped and antimony doped tin oxide films, Cryst. Res. Technol. 34 (1999) 1037–1046, https://doi.org/10.1002/(SICI)1521-4079(199909)34:8<1037::AID-CRAT1037>3.0.CO;2-J.
[41] C. Sima, C. Grigoriu, S. Antohe, Comparison of the dye-sensitized solar cells performances based on transparent conductive ITO and FTO, Thin Solid Films 519 (2010) 595–597, https://doi.org/10.1016/j.tsf.2010.07.002.
[42] S. Sharma, A.M. Volosin, D. Schmitt, D.K. Seo, Preparation and electrochemical properties of nanoporous transparent antimony-doped tin oxide (ATO) coatings, J. Mater. Chem. A 1 (2013) 699–706, https://doi.org/10.1039/c2ta00002d.
[43] S. Geiger, O. Kasian, A.M. Mingers, K.J.J. Mayrhofer, S. Cherevko, Stability limits of tin-based electrocatalyst supports, Sci. Rep. 7 (2017) 1–7, https://doi.org/10.1038/s41598-017-04079-9.
[44] A. Korjenic, K.S. Raja, Electrochemical stability of fluorine doped tin oxide (FTO) coating at different pH conditions, J. Electrochem. Soc. 166 (2019) C169–C184, https://doi.org/10.1149/2.0811906jes.
[45] F. Chiavaioli, F. Baldini, S. Tombelli, C. Trono, A. Giannetti, Biosensing with optical fiber gratings, Nanophotonics 6 (2017) 663–679, https://doi.org/10.1515/nanoph-2016-0178.
[46] X. Fu, L. Liu, S. Huang, G. Fu, W. Jin, W. Bi, Simultaneous measurement of temperature and refractive index with F–P microcavity sensor based on graded-index few mode fiber, Opt. Commun. 455 (2020), 124577, https://doi.org/10.1016/j.optcom.2019.124577.
[47] P. Sezemsky, D. Burnat, J. Kratochvil, H. Wulff, A. Kruth, K. Lechowicz, M. Janik, R. Bogdanowicz, M. Cada, Z. Hubicka, P. Niedziałkowski, W. Białobrzeska, V. Stranak, M. Śmietana, Tailoring properties of indium tin oxide thin films for their work in both electrochemical and optical label-free sensing systems, Sens. Actuators B Chem. 343 (2021), 130173, https://doi.org/10.1016/J.SNB.2021.130173.
[48] M. Piestrzyńska, M. Dominik, K. Kosiel, M. Janczuk-Richter, K. Szot-Karpińska, E. Brzozowska, L. Shao, J. Niedziółka-Jonsson, W.J. Bock, M. Śmietana, Ultrasensitive tantalum oxide nano-coated long-period gratings for detection of various biological targets, Biosens. Bioelectron. 133 (2019) 8–15, https://doi.org/10.1016/J.BIOS.2019.03.006.
[49] F. Khalilzadeh-Rezaie, I. Rezadad, I.O. Oladeji, J. Nath, J.W. Cleary, N. Nader, R. E. Peale, Fluorine-doped tin oxides for mid-infrared plasmonics, Opt. Mater. Express 5 (2015) 2184–2192, https://doi.org/10.1364/OME.5.002184.
[50] M.R. Shah, M.K. Alam, M.R. Karim, M.A. Sobhan, Study of optical properties of indium oxide (In2O3) thin films, in: Int. Conf. Mech. Eng., 2005: pp. 28–30. https://me.buet.ac.bd/icme/icme2005/Proceedings/PDF/ICME05-TH-10.pdf (Accessed December 1, 2021).
[51] M.M. El-Nahass, E.M. El-Menyawy, Thickness dependence of structural and optical properties of indium tin oxide nanofiber thin films prepared by electron beam evaporation onto quartz substrates, Mater. Sci. Eng. B Solid State Mater. Adv. Technol. 177 (2012) 145–150, https://doi.org/10.1016/j.mseb.2011.10.018.
[52] P. Prathap, Y.P.V. Subbaiah, M. Devika, K.T.R. Reddy, Optical properties of In2O3 films prepared by spray pyrolysis, Mater. Chem. Phys. 100 (2006) 375–379, https://doi.org/10.1016/j.matchemphys.2006.01.016.

[53] T.S. Sathiaraj, Effect of annealing on the structural, optical and electrical properties of ITO films by RF sputtering under low vacuum level, Microelectron. J. 39 (2008) 1444–1451, https://doi.org/10.1016/j.mejo.2008.06.081.
[54] Y.-H. Wang, K.H. Rahman, C.-C. Wu, K.-C. Chen, A review on the pathways of the improved structural characteristics and photocatalytic performance of titanium dioxide (TiO2) thin films fabricated by the magnetron-sputtering technique, Catalysts 10 (2020) 598, https://doi.org/10.3390/catal10060598.
[55] M. Śmietana, M. Myśliwiec, P. Mikulic, B.S. Witkowski, W.J. Bock, Capability for fine tuning of the refractive index sensing properties of long-period gratings by atomic layer deposited Al2O3 overlays, Sensors 13 (2013) (2013) 16372–16383, https://doi.org/10.3390/S131216372.
[56] I. Del Villar, C.R. Zamarreño, M. Hernaez, P. Sanchez, F.J. Arregui, I.R. Matias, Generation of surface plasmon resonance and lossy mode resonance by thermal treatment of ITO thin-films, Opt. Laser Technol. 69 (2015) 1–7, https://doi.org/10.1016/J.OPTLASTEC.2014.12.012.
[57] L.J. Meng, F. Placido, Annealing effect on ITO thin films prepared by microwave-enhanced dc reactive magnetron sputtering for telecommunication applications, Surf. Coat. Technol. 166 (2003) 44–50, https://doi.org/10.1016/S0257-8972(02)00767-3.
[58] V.A. Volpyas, A.Y. Komlev, R.A. Platonov, A.B. Kozyrev, Thermalization of the flow of sputtered target atoms during ion-plasma deposition of films, Phys. Lett. A 378 (2014) 3182–3184, https://doi.org/10.1016/J.PHYSLETA.2014.09.014.
[59] M. Śmietana, M. Dudek, M. Koba, B. Michalak, Influence of diamond-like carbon overlay properties on refractive index sensitivity of nano-coated optical fibres, Phys. Status Solidi 210 (2013) 2100–2105, https://doi.org/10.1002/PSSA.201300059.
[60] O. Fuentes, I. Del Villar, J.M. Corres, I.R. Matias, Lossy mode resonance sensors based on lateral light incidence in nanocoated planar waveguides, Sci. Rep. 9 (2019) 1–10, https://doi.org/10.1038/s41598-019-45285-x.
[61] M. Śmietana, P. Niedziałkowski, W. Białobrzeska, D. Burnat, P. Sezemsky, M. Koba, V. Stranak, K. Siuzdak, T. Ossowski, R. Bogdanowicz, Study on combined optical and electrochemical analysis using indium-tin-oxide-coated optical fiber sensor, Electroanalysis 31 (2019) 398–404, https://doi.org/10.1002/elan.201800638.
[62] K.S. Tseng, Y.L. Lo, Effect of sputtering parameters on optical and electrical properties of ITO films on PET substrates, Appl. Surf. Sci. 285 (2013) 157–166, https://doi.org/10.1016/J.APSUSC.2013.08.024.
[63] V. Stranak, R. Bogdanowicz, P. Sezemsky, H. Wulff, A. Kruth, M. Smietana, J. Kratochvil, M. Cada, Z. Hubicka, Towards high quality ITO coatings: the impact of nitrogen admixture in HiPIMS discharges, Surf. Coat. Technol. 335 (2018) 126–133, https://doi.org/10.1016/J.SURFCOAT.2017.12.030.
[64] E. Feigenbaum, K. Diest, H.A. Atwater, Unity-order index change in transparent conducting oxides at visible frequencies, Nano Lett. 10 (2010) 2111–2116, https://doi.org/10.1021/NL1006307.
[65] M. Śmietana, B. Janaszek, K. Lechowicz, P. Sezemsky, M. Koba, D. Burnat, M. Kieliszczyk, V. Stranak, P. Szczepański, Electro-optically modulated lossy-mode resonance, Nanophotonics 0 (2021), https://doi.org/10.1515/NANOPH-2021-0687.
[66] A.S. Cuharuc, G. Zhang, P.R. Unwin, Electrochemistry of ferrocene derivatives on highly oriented pyrolytic graphite (HOPG): quantification and impacts of surface adsorption, Phys. Chem. Chem. Phys. 18 (2016) 4966–4977, https://doi.org/10.1039/C5CP06325F.
[67] N. Kurapati, P. Pathirathna, R. Chen, S. Amemiya, Voltammetric measurement of adsorption isotherm for ferrocene derivatives on highly oriented pyrolytic graphite, Anal. Chem. 90 (2018) 13632–13639, https://doi.org/10.1021/acs.analchem.8b03883.
[68] S.Y. Tan, J. Zhang, A.M. Bond, J.V. Macpherson, P.R. Unwin, Impact of adsorption on scanning electrochemical microscopy voltammetry and implications for nanogap measurements, Anal. Chem. 88 (2016) 3272–3280, https://doi.org/10.1021/acs.analchem.5b04715.
[69] J.C. Zuaznabar-Gardona, A. Fragoso, Electrochemical characterisation of the adsorption of ferrocenemethanol on carbon nano-onion modified electrodes, J. Electroanal. Chem. 871 (2020), 114314, https://doi.org/10.1016/J.JELECHEM.2020.114314.
[70] D. Mampallil, K. Mathwig, S. Kang, S.G. Lemay, Reversible adsorption of outer-sphere redox molecules at Pt electrodes, J. Phys. Chem. Lett. 5 (2014) 636–640, https://doi.org/10.1021/jz402592n.
[71] H. Sato, I. Kusudo, M. Sugiyama, T. Hanasaki, N. Nakamura, Mössbauer spectroscopic study of ferrocene derivatives in the adsorption and liquid-crystalline states, Hyperfine Interact. 93 (1994) 1585–1590, https://doi.org/10.1007/BF02072913.
[72] I. Azcarate, C. Costentin, C. Methivier, C. Laberty-Robert, A. Grimaud, Electron transfer at the metal oxide/electrolyte interface: a simple methodology for quantitative kinetics evaluation, J. Phys. Chem. C 122 (2018) 12761–12770, https://doi.org/10.1021/acs.jpcc.8b02289.
[73] J.E. Carrera-Crespo, I. Fuentes-Camargo, R.E. Palma-Goyes, U.M. García-Pérez, J. Vazquez-Arenas, I. Chairez, T. Poznyak, Unrevealing the effect of transparent fluorine-doped tin oxide (FTO) substrate and irradiance configuration to unmask the activity of FTO-BiVO4 heterojunction, Mater. Sci. Semicond. Process. 128 (2021), 105717, https://doi.org/10.1016/J.MSSP.2021.105717.
[74] Y. Zhou, Z. Liu, C. He, C. Yin, Evolution of defects and charge carrier transport mechanism in fluorine-doped tin oxide thin films upon thermal treatment, J. Appl. Phys. 130 (2021), 135702, https://doi.org/10.1063/5.0062931.
[75] Z. Ma, Z. Li, K. Liu, C. Ye, V.J. Sorger, Indium-tin-oxide for high-performance electro-optic modulation, Nanophotonics 4 (2015) 198–213, https://doi.org/10.1515/NANOPH-2015-0006.
[76] L.H. Lalasari, T. Arini, L. Andriyah, F. Firdiyono, A.H. Yuwono, Electrical, optical and structural properties of FTO thin films fabricated by spray ultrasonic nebulizer technique from SnCl4 precursor, AIP Conf. Proc. 1964,2018. 020001. https://doi.org/10.1063/1.5038283.
[77] H.Z. Asl, S.M. Rozati, High-quality spray-deposited fluorine-doped tin oxide: effect of film thickness on structural, morphological, electrical, and optical properties, Appl. Phys. A Mater. Sci. Process. 125 (2019) 1–8, https://doi.org/10.1007/s00339-019-2943-8.
[78] M. Sobaszek, D. Burnat, P. Sezemsky, V. Stranak, R. Bogdanowicz, M. Koba, K. Siuzdak, M. Śmietana, Enhancing electrochemical properties of an ITO-coated lossy-mode resonance optical fiber sensor by electrodeposition of PEDOT:PSS, Opt. Mater. Express 9 (2019) 3069–3078, https://doi.org/10.1364/OME.9.003069.
[79] L. Jiang, H. Yu, L. Shi, Y. Zhao, Z. Wang, M. Zhang, S. Yuan, Optical band structure and photogenerated carriers transfer dynamics in FTO/TiO2 heterojunction photocatalysts, Appl. Catal. B Environ. 199 (2016) 224–229, https://doi.org/10.1016/J.APCATB.2016.05.070.
[80] C.J. Van Oss, R.F. Giese, P.M. Bronson, A. Docoslis, P. Edwards, W.T. Ruyechan, Macroscopic-scale surface properties of streptavidin and their influence on aspecific interactions between streptavidin and dissolved biopolymers, Coll. Surf. B Biointerfaces 30 (2003) 25–36, https://doi.org/10.1016/S0927-7765(03)00025-0.
[81] D. Basnig, N. Vilá, G. Herzog, A. Walcarius, Voltammetric behaviour of cationic redox probes at mesoporous silica film electrodes, J. Electroanal. Chem. 872 (2020), 113993, https://doi.org/10.1016/J.JELECHEM.2020.113993.

Dariusz Burnat received a B.Sc. and M.Sc. degree from Warsaw University of Technology, Poland, in 2015 and 2018, respectively. Currently, he is working towards a Ph.D. degree in the Institute of Microelectronics and Optoelectronics, Warsaw University of Technology. His research interests include sputtered thin films for optical fiber sensors.

Petr Sezemsky is a Ph.D. student at the University of South Bohemia in branch of Biophysics. His work is focused on research and deposition of bioactive and biofunctional surfaces. His field of interest is low-temperature plasma deposition, bio-functional and antibacterial surfaces, sensor technique.

Katarzyna Lechowicz received a B.Sc. and M.Sc. degree from Warsaw University of Technology, Poland in 2019 and 2021, respectively. Currently, she is working towards a Ph.D. degree in the Institute of Microelectronics and Optoelectronics, Warsaw University of Technology. His research interests include transparent oxides for optical fiber and electrochemical sensors.

Marcin Koba received a M.Sc. degree in optoelectronics in 2006, and Ph.D. and D.Sc. degrees in electronics in 2011 and 2017, respectively, all from the Warsaw University of Technology, Warsaw, Poland. His current interests include laser physics, solid-state physics, optical communication, photonics, fiber-optic sensing structures and metrology.

Marta Janczuk-Richter received her M.Sc. in biotechnology from the Warsaw University of Technology, Poland in 2014 and Ph.D. in chemistry from the Institute of Physical Chemistry, Polish Academy of Sciences. Her research interests are biosensors based on optical fibers, surface functionalization for biosensor development and utilization of bacteriophages as sensing elements.

Monika Janik received the B.Sc. and M.Sc. degrees in biotechnology from the Wroclaw University of Science and Technology, Poland, in 2014 and 2015, respectively. In 2019 she received a Ph.D. degree in photonics from the Universite du Quebec en Outaouais, Canada. Her current interests include designing and optimizing different kinds of biosensors.

Vitezslav Stranak received a Ph.D. from the Charles University in Prague, Czech Republic in 2007. Afterwards he was a postdoctoral fellow in Greifswald (Germany) oriented on low-temperature plasma diagnostics and deposition of thin film. Since 2013 he is with University of South Bohemia, Czech Republic as associated professor performing applied research of thin nanostructured and functional thin films.

Joanna Niedziółka-Jönsson received her M.Sc. in chemistry from the Warsaw University of Technology, Poland in 2000 and Ph.D in chemistry from the Institute of Physical Chemistry, Polish Academy of Sciences where she is presently working as a professor. Since Jan 2012 she leads the Surface Nanoengineering research group. Her scientific interests are surface functionalisation for optical and electro-chemical sensors.

Robert Bogdanowicz received his Ph.D. degree (with distinction) in Electronics from the Gdansk University of Technology in 2009. His current domains of interest include selective CVD diamond growth and nanocrystalline diamond doping for environmental and biochemical nanosensors. In 2015 he held a scholarship Fulbright Senior Scholar Program at the California Institute of Technology (Caltech) in the group of prof. William Goddard (Materials and Process Simulation Center) working on hybrid 3D diamond structures.

Mateusz Śmietana received his B.Sc., M.Sc., Ph.D. (with distinction), and D.Sc. degrees in electronics from the Warsaw University of Technology (WUT), Poland, in 2000, 2002, 2007, and 2014, respectively. Since December 2015, he has been an Associate Professor in the Institute of Microelectronics and Optoelectronics, WUT. He was a postdoctoral fellow at Virginia Tech, USA and Université du Québec en Outaouais, Canada, as well as a visiting professor at Southern University of Science and Technology (China). He has authored and

co-authored more than 150 scientific papers. His fields of interest are fiber-optic sensors and thin films.